

# New methods for computing the generalized chi-square distribution

Abhramil Das

abhramil.das@utexas.edu

Center for Perceptual Systems, and Center for Theoretical and Computational Neuroscience  
The University of Texas at Austin

April 9, 2024

## Abstract

We present several exact and approximate mathematical methods and open-source software to compute the cdf, pdf and inverse cdf of the generalized chi-square distribution, which appears in Bayesian classification problems. Some methods are geared for speed, while others are designed to be accurate far into the tails, using which we can also measure large values of the discriminability index  $d'$  between multinormals. We compare the accuracy and speed of these methods against the best existing methods.

which we can simply differentiate to obtain an expression for the pdf as a sum of chi-square pdf's:

$$f(x) = \frac{1}{\beta} \sum_{i=0}^{\infty} a_i f_{\chi_{d+2i}^2}(x/\beta).$$

These can be used by calling `gx2cdf(..., 'method', 'ruben')` and `gx2pdf(..., 'method', 'ruben')` in our Matlab toolbox '[Generalized chi-square distribution](#)' (source code [on github](#)).

Imhof<sup>22</sup> used Gil-Pelaez's method<sup>23</sup> of inverting the characteristic function to compute the cdf and pdf for mixed  $w_i$  as well, but not with the normal term. Davies<sup>24</sup> extended the characteristic function to let Imhof's inversion work with the normal  $s$  term too, and we further incorporated the offset  $m$  and implemented it as `gx2cdf(..., 'method', 'imhof')` and `gx2pdf(..., 'method', 'imhof')` in our toolbox. We provide the option to compute the required integral fast with double precision numerics, or slowly but more accurately using variable precision arithmetic (vpa).

These methods all work well in the center of the distribution, but far into the tails they begin to reach their limits of accuracy or speed at different points. For this reason several approximations have been derived for the cdf, such as Imhof's extension<sup>22</sup> of Pearson's approximation<sup>25</sup> (only usable when  $s = 0$ ), and Liu et al's<sup>26</sup> and Zhang et al's<sup>27</sup> approximations (only usable when  $\mathbf{q}_1 = 0$ , i.e.  $s = 0$ , and  $\mathbf{Q}_2$  is non-negative definite, i.e. when all  $w_i$  are the same sign). These approximate methods are often only applicable to limited cases, and even then have their inaccuracies. See Zhang et al,<sup>27</sup> Duchesne et al<sup>28</sup> and Bodenham et al<sup>29</sup> for a review of these approximate methods and their limitations.

In this paper our aim is to develop several new methods to compute the generalized chi-square cdf, pdf and inverse cdf. These methods will have different tradeoffs, e.g. the inverse Fourier transform method is geared for speed, the ray-trace method is slower but accurate far into the tails, and the ellipse method is a fast approximation that becomes exact in the finite tail.

## 2 Mapping to a quadratic form

We had previously shown how to map from the parameters of a multinormal and the coefficients of its quadratic form to the parameters of the resulting generalized chi-square distribution<sup>7</sup> (function `norm_quad_to_gx2_params` in our toolbox). As a first

## 1 Introduction

The generalized chi-square variable  $\tilde{\chi}$  is a quadratic form of a  $d$ -dimensional multinormal variable  $\mathbf{x} \sim N(\boldsymbol{\mu}, \boldsymbol{\Sigma})$ , and can also be seen as a weighted sum of non-central chi-square variables  $\chi'^2$  and a standard normal variable  $z$ :

$$\begin{aligned} \tilde{\chi}_{\mathbf{w}, \mathbf{k}, \boldsymbol{\lambda}, s, m} &= q(\mathbf{x}) = \mathbf{x}' \mathbf{Q}_2 \mathbf{x} + \mathbf{q}_1' \mathbf{x} + q_0 \\ &= \sum_i w_i \chi_{k_i, \lambda_i}^{\prime 2} + sz + m. \end{aligned}$$

(Regular symbols are scalars, bold lowercase symbols are column vectors, and bold uppercase symbols are matrices.)

This distribution arises across many fields, such as statistics and machine learning,<sup>1–6</sup> neuroscience,<sup>7</sup> cosmology,<sup>8,9</sup> signal transmission,<sup>10–12</sup> satellite navigation,<sup>13,14</sup> quality control,<sup>15</sup> cybersecurity<sup>16</sup> and robotics.<sup>17–20</sup>

When  $s = 0$  and  $w_i$  are all positive or all negative, the distribution starts from the finite point  $m$  at one end, which can be called a finite tail, and the other end tails off at  $+\infty$  or  $-\infty$  respectively, which we call an infinite tail. When  $w_i$  have mixed signs, and/or there is a normal  $s$  term, both tails are infinite.

There are several existing methods to compute the cdf and pdf of this distribution, which sometimes behave differently in finite vs. infinite tails. When all  $w_i$  are the same sign and there is no linear normal term ( $s = 0$ ), Ruben's method<sup>21</sup> can be used to compute the cdf as a sum of chi-square cdf's:

$$F(x) = \sum_{i=0}^{\infty} a_i F_{\chi_{d+2i}^2}(x/\beta),$$

step to some of our methods, it will help to find the inverse map, i.e. from the parameters of a generalized chi-square distribution to the parameters of a multinormal and its quadratic form. This inverse map is one-to-many: there are infinite pairs of multinormals and corresponding quadratics that have the same distribution. So, in order to arrive at a single solution, we shall consider a canonical form where the multinormal is the standard normal, and find a quadratic form of it that will produce the given generalized chi-square distribution.

Let us start from an example. Suppose the generalized chi-square parameters are weights  $\mathbf{w} = [w_1 \ w_2 \ w_3]$ , degrees of freedom  $\mathbf{k} = [1 \ 1 \ 2]$ , non-centralities  $\boldsymbol{\lambda} = [\lambda_1 \ \lambda_2 \ \lambda_3]$ , and linear coefficients  $s$  and  $m$ . We build this as a sum of squares of independent scaled and shifted standard normal variables  $z_i$ , plus a linear term. For any term with multiple degrees of freedom, we split it into as many standard normals, choosing to put the entire non-centrality in the first term. So in this case we have the quadratic as:

$$q(\mathbf{z}) = w_1(z_1 - \sqrt{\lambda_1})^2 + w_2(z_2 - \sqrt{\lambda_2})^2 + w_3\{(z_3 - \sqrt{\lambda_3})^2 + z_4^2\} + sz_5 + m. \quad (1)$$

Now let us express the quadratic in vector and matrix notation:  $q(\mathbf{z}) = \mathbf{z}'\mathbf{Q}_2\mathbf{z} + \mathbf{q}'_1\mathbf{z} + q_0$ , where  $\mathbf{z}$  is a standard normal vector,  $\mathbf{Q}_2$  is a square matrix, and  $\mathbf{q}_1$  is a vector. First consider  $s = 0$ . Then the standard normal has  $\sum k_i$  dimensions. Collecting the second order terms, we can see that the matrix  $\mathbf{Q}_2$  is diagonal, here  $[w_1 \ w_2 \ w_3 \ w_3]$ , i.e. in general it is constructed by appending each  $w_i$   $k_i$  times. Then collecting the linear  $z_i$  terms, we see that  $\mathbf{q}'_1 = [-2w_1\sqrt{\lambda_1} \ -2w_2\sqrt{\lambda_2} \ -2w_3\sqrt{\lambda_3} \ 0]$ , i.e. in general we append each  $-2w_i\sqrt{\lambda_i}$ , followed by a 0  $k_i - 1$  times. And  $q_0 = \sum w_i\lambda_i + m$ . Now when  $s \neq 0$ , we increase the dimension to  $\sum k_i + 1$ , append the diagonal  $\mathbf{Q}_2$  with a 0, and append  $\mathbf{q}_1$  with  $s$ . This mapping is available as function `gx2_to_norm_quad_params` in our toolbox.

Given any quadratic form of any multinormal, we can simplify it by first finding its generalized chi-square parameters, then mapping back to this canonical quadratic of the standard multinormal.

Even though in this inverse map we fix the multinormal to be the unit sphere, this is still not its only quadratic function that has the given distribution. What is the entire family of inverse maps? First, in a term with multiple degrees of freedom, we could split the total non-centrality in any way, which corresponds to rotating the quadratic around the origin in that sub-space. Second, we can apply any linear transform to the entire space where the multinormal and the quadratic lives. So we can spherically rotate the quadratic around the origin without changing the distribution, and finally we can scale and shift the space so that the multinormal is no longer standard.

By mapping from generalized chi-square parameters to quadratic coefficients, then sampling standard normal vectors and computing their quadratic form, we can sample from the generalized chi-square distribution (function `gx2rnd` in our toolbox). This is an alternative to sampling from the constituent noncentral chi-squares and a normal and adding them.

Fig. 1a shows the cdf of a generalized chi-square distribution with  $\mathbf{w} = [1 \ -1]$ ,  $\mathbf{k} = [1 \ 1]$ ,  $\boldsymbol{\lambda} = [2 \ 4]$ ,  $s = m = 0$ . To compute the cdf, we first map these parameters to the cor-

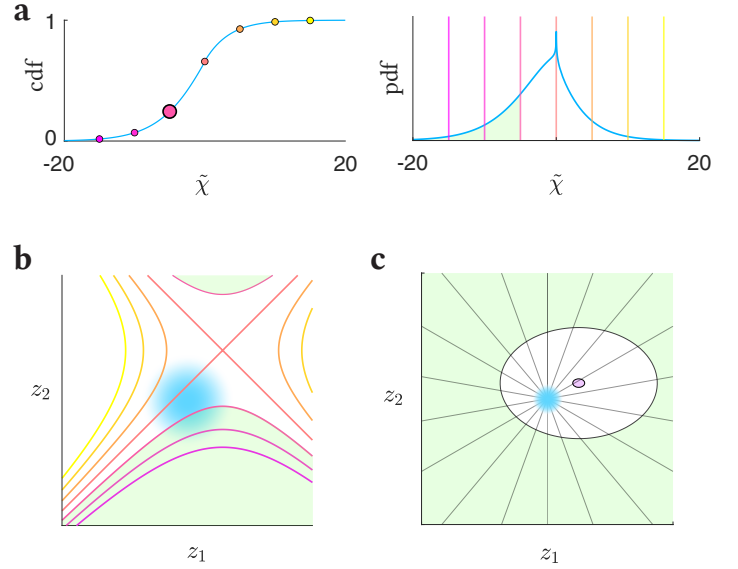


**Figure 1:** Mapping from the generalized chi-square parameters to the quadratic form of a multinormal, and integrating using ray-trace. **a.** A generalized chi-square cdf at one of several points (left, larger dot) is the pdf integrated up to that point (right, green area). **b.** This integrated probability corresponds to the standard multinormal (blue blob) probability over a domain (green area) that belongs to a family of quadratics (colours in this family correspond across plots a-b). **c.** The cdf of a generalized chi-square with all positive  $\mathbf{w}$  in the lower (finite) and upper (infinite) tails corresponds to the standard multinormal (blue blob) probability inside the tiny ellipse (purple area) and outside the large ellipse (green area) respectively. All rays emanating from the normal hit the large ellipse, but most miss the small one.

responding quadratic form of a bivariate standard normal,  $\tilde{\chi} = q(\mathbf{z}) = z_1^2 - z_2^2 - 2\sqrt{2}z_1 + 4z_2 - 2$ , a hyperbolic function. The cdf at a point  $F(c) = p(\tilde{\chi} < c) = p(q(\mathbf{z}) < c)$  is the multinormal probability within the contour of  $q(\mathbf{z})$  at level  $c$ , i.e. the green area defined by the hyperbola  $q(\mathbf{z}) < c$  or  $q(\mathbf{z}) - c < 0$ , fig. 1b. The cdf at other points are the probabilities within the other hyperbolas in this family as we vary  $c$ . These probabilities can be integrated in the  $\mathbf{z}$ -space with the ray-tracing method, as described in the following section.

## 3 Ray-tracing

### 3.1 Computing the cdf

Once we map from the generalized chi-square parameters to the quadratic form of a standard normal vector, we can now use the ray-tracing method<sup>7</sup> to compute the cdf, available in our toolbox as `gx2cdf(..., 'method', 'ray')`. This is a method to compute the multinormal probability over arbitrary domains, including quadratic domains, for which it is especially fast and accurate. In this method, we first linearly transform the space so that the distribution is the standard (unit spherical) multinormal. Then we send 'rays' out from its center at every angle, and find the distances where each ray hits the integration domain. Using this we analytically integrate the density along each ray, which we then numerically integrate across all the rays. In Matlab we can use

grid integration across rays for up to 4 dimensions, and Monte-Carlo integration above that (or even in general), which automatically runs in parallel on a GPU when present.

The ray method uses careful strategies to preserve precision and compute probabilities down to about  $10^{-308}$ , the smallest value expressible in double precision (called `realmin`). This is already a small enough probability for most imaginable applications. But for those beyond imagination, we provide a `vpa` option that can be turned on to implement the calculations symbolically, and evaluate the result with variable precision. (This works only with Monte-Carlo integration across rays, not with Matlab's native grid integration.) When the `vpa` setting is off, if the method detects rays that cross the integration domain, yet the double-precision probability on them are 0, it notifies the user to turn on `vpa` if they want to include those small probabilities. With this, the ray-tracing can be extended to compute probabilities smaller than `realmin`, all the way down to the absurdly small scale of about  $10^{-3 \times 10^8}$ , where Matlab's symbolic calculation engine fails, so let us call this `symmin`. Just as Bill Gates allegedly said in 1981 that nobody should need more than 640KB of computer memory, we too believe that nobody should ever need this level of precision.

However, the ray method can reach such small tail probabilities only in the infinite tails of a generalized chi-square distribution. When all  $w_i$  are the same sign and  $s = 0$ , the distribution has one finite tail, and the corresponding quadratic form is an ellipse. For example, consider  $\tilde{\chi} = 2\chi_{k=1, \lambda=4}'^2 + 4\chi_{k=1, \lambda=1}'^2$ . This corresponds to an elliptical quadratic form:  $\tilde{\chi} = q(\mathbf{z}) = 2(z_1 - 2)^2 + 4(z_2 - 1)^2$  of the bivariate standard normal (fig. 1c). The lower (finite) tail probability  $F(c) = p(q(\mathbf{z}) < c)$ , where  $c$  is small, is the standard normal probability inside a tiny offset elliptical region (purple area), whereas the upper (infinite) tail probability  $p(\tilde{\chi} > c)$ , where  $c$  is large, is the probability outside a large elliptical region (green area). When we send rays from the normal center to compute the upper tail probability, they all hit the large domain and return small values that accurately sum to the small upper tail probability. But in the lower tail, most rays miss the tiny elliptical domain. If the domain is very tiny, no ray may hit it, and the cdf will be incorrectly computed as 0. In  $\leq 4$  dimensions, Matlab's adaptive grid integral can, to some extent, automatically find the tiny domain and populate the grid densely there and avoid this problem, but beyond 4 dimensions, randomly sampled Monte-Carlo rays will all miss a small enough domain. Therefore, the ray method is better for infinite tails.

### 3.2 Computing the pdf

The ray-tracing method, which we developed to compute the cdf of any function  $f(\mathbf{x})$  of a normal vector  $\mathbf{x} \sim N(\boldsymbol{\mu}, \boldsymbol{\Sigma})$ , can also be modified to compute the pdf. A simple way to compute the pdf at  $c$  is to compute the cdf at two nearby points  $c \pm \Delta c$ , and finite-difference them numerically. However, numerical differentiation is slower because it requires two evaluations of the cdf, and has limited accuracy when we need to differentiate finely. We present here the calculations to do this differentiation analytically instead, which extends the ray-tracing method to be able to compute densities of arbitrary functions of normal random vectors with greater speed and accuracy.

In the ray method, we first linearly transform the space so that the multinormal becomes the standard normal  $\mathbf{z}$ , and the function is transformed to the *standardized* function in this space:  $\tilde{f}(\mathbf{z}) = f(\mathbf{S}\mathbf{z} + \boldsymbol{\mu})$ , where  $\mathbf{S} = \boldsymbol{\Sigma}^{\frac{1}{2}}$  is the symmetric square root. Similar to fig. 1 of our ray-tracing paper<sup>7</sup> and corresponding explanations, fig. 4a here illustrates a ray sent from the origin (black dot) of this  $d$ -dimensional standard multinormal in the direction of a unit vector  $\mathbf{n}$ .  $z$  is the coordinate along the ray, so that the vector location of point  $\mathbf{z}$  on the ray is  $\mathbf{z} = \mathbf{n}z$  in the full space. The blue distribution  $\phi_d^{\text{ray}}(z) = f_{\chi_d}(|z|)/2$  ( $f_{\chi_d}$  is the chi distribution pdf) is the density of the standard multinormal along the ray, and  $\tilde{f}_{\mathbf{n}}(z)$  is the value of the function  $\tilde{f}$  along the ray.

Now, to find the pdf of  $f(\mathbf{x})$  at  $c$ , we need to know the probability that  $f(\mathbf{x})$ , or  $\tilde{f}(\mathbf{z})$  in the standardized space, is between  $c$  and  $c + dc$ . This is the probability that the  $\tilde{f}_{\mathbf{n}}(z)$  along each ray  $\mathbf{n}$  is between  $c$  and  $c + dc$ , summed across all rays. Fig. 4a shows this horizontal slice. The probability that  $\tilde{f}_{\mathbf{n}}(z)$  is within this slice is the probability of finding  $z$  within the corresponding vertical slices at  $z_1, z_2$  or  $z_3$  (the roots of  $\tilde{f}_{\mathbf{n}}(z) - c$ ), given by  $dp(\mathbf{n}) = \sum_i \phi_d^{\text{ray}}(z_i) |dz_i|$ , where  $|dz_i|$  is the width of each vertical slice, which can be found from the slope of the function:  $|\tilde{f}'_{\mathbf{n}}(z_i)| = dc/|dz_i| \implies |dz_i| = dc/|\tilde{f}'_{\mathbf{n}}(z_i)|$ . So we have  $dp(\mathbf{n}) = \sum_i \phi_d^{\text{ray}}(z_i) / |\tilde{f}'_{\mathbf{n}}(z_i)| dc$ . Now to integrate this across directions  $\mathbf{n}$ , we need to weight each  $dp(\mathbf{n})$  by the volume fraction of the double-cone subtended by the differential angle element  $d\mathbf{n}$ , which is  $\frac{2d\mathbf{n}}{\Omega_d}$  ( $\Omega_d$  is the total angle in  $d$  dimensions), then sum. Since this gives us the probability that  $f$  is between  $c$  and  $c + dc$ , dividing away  $dc$  then gives us the probability density:

$$\frac{2}{\Omega_d} \int_{\Omega_d/2} \underbrace{\sum_i \frac{\phi_d^{\text{ray}}(z_i)}{|\tilde{f}'_{\mathbf{n}}(z_i)|}}_{\alpha(\mathbf{n})} d\mathbf{n}$$

For up to four dimensions, the integral is carried out numerically across half the total angle (since the probability on each ray already accounts for both directions of the ray). Beyond that, we perform a Monte Carlo integration, which finds the average value  $\bar{\alpha}$  of the integrand over the *total* angle  $\Omega_d$ , which is  $\alpha(\mathbf{n})$  integrated over  $\Omega_d$ , divided by  $\Omega_d$ . Since the integral of  $\alpha(\mathbf{n})$  over  $\Omega_d$  is double that over  $\Omega_d/2$ , this automatically provides the extra factor of 2 needed to match the above equation.

Note that instead of inefficiently numerically computing the slope  $\tilde{f}'_{\mathbf{n}}(z)$ , we can see that it is simply the gradient of  $\tilde{f}(\mathbf{z})$  in the direction  $\mathbf{n}$ :  $\tilde{f}'_{\mathbf{n}} = \mathbf{n} \cdot \nabla \tilde{f}$ . This still needs the gradient of the standardized function, but we can only expect the user to supply the gradient of the original function  $f$ . Fortunately, we can relate  $\nabla \tilde{f}$  to  $\nabla f$ . Remembering that  $\tilde{f}(\mathbf{z}) = f(\mathbf{x})$ , where  $\mathbf{x} = \mathbf{S}\mathbf{z} + \boldsymbol{\mu}$ , i.e.  $x_j = \sum_i S_{ji} z_i + \mu_j$ , we can write:

$$\begin{aligned} \nabla_i \tilde{f}(\mathbf{z}) &= \frac{\partial \tilde{f}(\mathbf{z})}{\partial z_i} = \frac{\partial f(\mathbf{x})}{\partial z_i} = \sum_j \frac{\partial f(\mathbf{x})}{\partial x_j} \frac{\partial x_j}{\partial z_i} \\ &= \sum_j \nabla_j f(\mathbf{x}) S_{ji} = \sum_j S'_{ij} \nabla_j f(\mathbf{x}). \end{aligned}$$

That is,  $\nabla \tilde{f}(\mathbf{z}) = \mathbf{S}' \nabla f(\mathbf{S}\mathbf{z} + \boldsymbol{\mu})$ . So, when  $f$  and  $\nabla f$  are both supplied, the pdf can be computed more quickly and accurately. This method is available as function `norm_fun_pdf` in our tool-

box 'Integrate and classify normal distributions' (source code on [github](#)).

Fig. 4b shows the pdf of a cubic function  $f(x) = x_1^3 + x_2^2 - x_3 x_4$  of a 4-dimensional normal:

$$\mathbf{x} \sim N(\boldsymbol{\mu}, \boldsymbol{\Sigma}), \quad \boldsymbol{\mu} = \begin{bmatrix} 4 \\ -2 \\ 3 \\ 2 \end{bmatrix}, \quad \boldsymbol{\Sigma} = \begin{bmatrix} 1 & 0 & -1 & 0 \\ 0 & 8 & 4 & 0 \\ -1 & 4 & 8 & 0 \\ 0 & 0 & 0 & 1 \end{bmatrix},$$

computed using three methods. There exists no other standard specialized method for computing pdf's of general functions of multinormals, so our baseline reference is a Monte-Carlo method where we sample normal vectors, compute their function values, then histogram them to estimate the pdf. With  $4 \times 10^7$  samples, this takes 1.8s per point, but does not reach too far into the tails. The ray-tracing method with numerical differencing uses only 2000 rays, and in a similar 1.9s per point reaches about 5 [todo get exact number] orders of magnitude deeper in the upper tail, and about 15 orders deeper in the lower tail, but is noisy due to numerical errors in the differencing. The analytical derivative method uses only 1000 rays, and in half the time, 1s per point, reaches even farther [todo x orders deeper] with greater accuracy. The remaining small noisy errors in the pdf are due to the Monte Carlo sampling of rays, and can be smoothed by growing the sample. Note the distinction from the vanilla Monte-Carlo method: In  $>4$  dimensions the ray method uses Monte-Carlo integration, but only across rays at different angles (the radial integral is computed analytically), so it converges much faster than using vanilla Monte-Carlo integration over all dimensions, as in the baseline method here.

Suppose we are using this method to find the pdf of a generalized chi-square distribution at the point  $c$ . Then we first find the corresponding quadratic  $q(z) = \mathbf{z}' \mathbf{Q}_2 \mathbf{z} + \mathbf{q}'_1 \mathbf{z} + q_0$  of the standard (multi)normal. Then for any ray in this space in the direction  $\mathbf{n}$ , the value of this function is a quadratic of the  $z$  coordinate along the ray:<sup>7</sup>

$$\begin{aligned} q_{\mathbf{n}}(z) &= q(z\mathbf{n}) = \mathbf{n}' \mathbf{Q}_2 \mathbf{n} z^2 + \mathbf{q}'_1 \mathbf{n} z + q_0 \\ &= q_2(\mathbf{n}) z^2 + q_1(\mathbf{n}) z + q_0. \end{aligned}$$

Now we find the roots of  $q_{\mathbf{n}}(z) - c = q_2 z^2 + q_1 z + q_0 - c$ . For there to exist two roots, we must have  $q_2 \neq 0$  and the discriminant  $\Delta = q_1^2 - 4q_2(q_0 - c) > 0$ . Along the rays where this holds, the roots are  $z_i = \frac{-q_1 \pm \sqrt{\Delta}}{2q_2}$ , and the slope of the quadratic is the same magnitude at either root:  $|q'(z_i)| = |2q_2 z_i + q_1| = \sqrt{\Delta}$ . And if  $q_2 = 0$  but  $q_1 \neq 0$ , then the function is a line with one root  $z = \frac{c - q_0}{q_1}$ , with slope magnitude  $|q_1| = \sqrt{\Delta}$  again. These give us the quantities which we then integrate across different rays, either by quadrature (upto 4D) or Monte-Carlo, to get the generalized chi-square pdf at  $c$ . In our Matlab implementation `gx2pdf(..., 'method', 'ray')`, we implement this using fast vector operations, and speed up the Monte-Carlo integration by using the same sample of rays to compute the pdf at multiple points.

## 4 Inverse Fourier transform

### 4.1 Computing the cdf

Arguably the best existing general method to compute the generalized chi-square cdf  $F(x)$  is Imhof's method,<sup>22</sup> which uses the Gil-Pelaez theorem<sup>23</sup> to write it as an integral involving the characteristic function  $\phi(t)$  (function `gx2char` in our toolbox):

$$F(x) = \frac{1}{2} - \frac{1}{\pi} \int_0^\infty \frac{\text{Im}[\phi(t) e^{-itx}]}{t} dt.$$

This integral is then carried out numerically to the requested tolerance, which sums the integrand over an adaptive grid to approximate the pdf at the single point  $x$ . However, let us follow a different path instead to get it to the form of a discrete inverse Fourier transform, starting from the Gil-Pelaez theorem:

$$\begin{aligned} F(x) &= \frac{1}{2} + \frac{1}{2\pi} \int_0^\infty \frac{\phi(-t) e^{itx} - \phi(t) e^{-itx}}{it} dt \\ &= \frac{1}{2} + \frac{1}{4\pi} \int_{-\infty}^\infty \frac{\phi(-t) e^{itx} - \phi(t) e^{-itx}}{it} dt \\ &= \frac{1}{2} + \frac{1}{2\pi} \int_{-\infty}^\infty \frac{\phi(-t)}{it} e^{itx} dt. \end{aligned}$$

This gets it into the form of a continuous inverse Fourier transform of the function  $\tilde{\phi}(t) = \phi(-t)/it$ . Now, suppose  $t_n = n\Delta t$ ,  $n = \{-N, \dots, N\}$  is a uniform grid from  $-N\Delta t$  to  $N\Delta t$ , with spacing  $\Delta t$ . If  $N\Delta t$  is large and  $\Delta t$  is small, then we can approximate the integral as a discrete sum:

$$F(x) \approx \frac{1}{2} + \frac{1}{2\pi} \sum_{n=-N}^N \tilde{\phi}(t_n) e^{it_n x} \Delta t.$$

Let's call  $\tilde{\phi}_n = \tilde{\phi}(t_n)$ . Now, suppose  $x_j = j\Delta x$ ,  $j = \{-N, \dots, N\}$  is a uniform grid of points. Substituting, we get:

$$F(x_j) \approx \frac{1}{2} + \frac{1}{2\pi} \sum_{n=-N}^N \tilde{\phi}_n e^{in\Delta t j\Delta x} \Delta t.$$

So if we select  $\Delta t = \frac{2\pi}{(2N+1)\Delta x}$ , this becomes:

$$F(x_j) \approx \frac{1}{2} + \frac{1}{\Delta x} \frac{1}{2N+1} \sum_{n=-N}^N \tilde{\phi}_n e^{2\pi i j n / (2N+1)} = \frac{1}{2} + \frac{\hat{\phi}_j}{\Delta x},$$

where  $\hat{\phi}_j$  is the discrete inverse Fourier transform of  $\tilde{\phi}_n$ . Most programming languages have optimized IFFT functions, using which we can find the value of the cdf at not one, but simultaneously the entire grid of points, at blazing fast speeds. Increasing the range of the grid and reducing the spacing  $\Delta x$  improves accuracy, but sacrifices speed. There is another trade-off: the cdf is returned only over a uniform grid of points, whereas the Imhof-Davies method can compute it at any specific point. To do this here with IFFT, we first evaluate it over a fine grid that surrounds those points, then interpolate to the given points, which is still quite fast. This method is available as `gx2cdf(..., 'method', 'ifft')` in our toolbox.



## 4.2 Computing the pdf

The best existing method to compute the generalized chi-square pdf in general is also Imhof's method,<sup>22</sup> which can be arrived at by differentiating the cdf expression, yielding:

$$f(x) = \frac{1}{\pi} \int_0^\infty \operatorname{Re}[\phi(t) e^{-itx}] dt.$$

Similar to the case of the cdf, we shall instead try to change this to a discrete inverse Fourier transform, starting from the basic inversion formula:

$$f(x) = \frac{1}{2\pi} \int_{-\infty}^\infty \phi(t) e^{-itx} dt = \frac{1}{2\pi} \int_{-\infty}^\infty \phi(-t) e^{itx} dt.$$

This is a continuous inverse Fourier transform of the function  $\tilde{\phi}(t) = \phi(-t)$ . Following our previous derivation, we can approximate this as:

$$f(x_j) \approx \frac{\hat{\phi}_j}{\Delta x},$$

where  $\hat{\phi}_j$  is the discrete inverse Fourier transform of  $\tilde{\phi}_n = \tilde{\phi}(t_n)$ .

This method is available as `gx2pdf(..., 'method', 'ifft')` in our toolbox.

## 5 Finite-tail ellipse approximation

### 5.1 Computing the cdf

As we mentioned in the introduction, the generalized chi-square distribution has a finite tail when  $w_i$  are all the same sign and  $s = 0$ . For example, consider all positive  $w_i$  and  $s = m = 0$ . The lower tail at 0 here is such a finite tail. Imhof's method, and as we discussed, the ray method, are not very good at computing small cdf values in this tail. Ruben's method<sup>21</sup> performs better in this tail, and can reach down to `realmin` pretty fast, below which it returns 0. In this section we show a simple approximation that can also be used for such finite tails, which can reach much lower and also becomes exact in that limit.

Note that in this case the quadratic form corresponding to the distribution is an ellipse (or an ellipsoid or hyper-ellipsoid in general), that gets vanishingly small as we approach the end of the tail, e.g. the purple ellipse in fig. 1c. The cdf is given by the probability inside this ellipse:

$$F(x) = p \left( \sum_{j=1}^d \omega_j (z_j - c_j)^2 < x \right).$$

The parameters of this ellipse can be easily identified once we write the quadratic form like in eq. 1. The ellipse is in  $d = \sum k_i$  dimensions, and its center  $c$  is the vector built by appending each  $\sqrt{\lambda_i}$  followed by a 0  $k_i - 1$  times. The weights  $\omega_j$  are the elements of the diagonal matrix  $\mathbf{Q}_2$  derived in sec. 2, formed by appending each  $w_i$   $k_i$  times. The semi-axis-lengths are  $a_j = \sqrt{x/\omega_j}$ .

A simple approximation for the probability inside this ellipse is to first compute the probability in the (hyper-) rectangle that encloses it (whose vertices are semi-axis-lengths above and below the center), using, say, Matlab's `mvncdf`, then multiplying it

by the ratio of the ellipse volume to the rectangle volume. The approximation here is that we take the average probability density over the ellipse to be the same as over the rectangle, which becomes increasingly accurate as we approach the tail end and the ellipse gets tinier. However, computing the probability in the rectangle has its own associated error, and it cannot even always reach `realmin` like Ruben's fast exact method can, so this approximation is not very useful.

An even simpler approximation is to multiply the multinormal probability density at the ellipse center  $c$ , with the ellipse volume:

$$\begin{aligned} \lim_{x \rightarrow 0} F(x) &= (2\pi)^{-\frac{d}{2}} e^{-\frac{\|c\|^2}{2}} \frac{\pi^{\frac{d}{2}} \sqrt{\prod_j \frac{x}{\omega_j}}}{\Gamma(\frac{d}{2} + 1)} \\ &= \frac{(x/2)^{\frac{d}{2}} e^{-\frac{\|c\|^2}{2}}}{\Gamma(\frac{d}{2} + 1) \sqrt{\prod_j \omega_j}}. \end{aligned} \quad (2)$$

So the cdf is simply proportional to a power of  $x$ . Here the approximation is that we take the average probability density over the ellipse to be the same as at its center, which again becomes more accurate as we approach the tail end.

This expression corresponds to the first term ( $j = k = 0$ ) of the power series expression of  $F(x)$  that Shah and Khatri<sup>30</sup> derived for this case, albeit not from a geometric interpretation such as this.

To better compute tiny cdf values at tiny  $x$  values, we can look at the log probability instead, which is simply linear in  $\log x$ :

$$\begin{aligned} \lim_{x \rightarrow 0} \log_{10} F(x) &= \frac{d}{2} (\log_{10} x - \log_{10} 2) - \frac{\|c\|^2}{\ln 100} \\ &\quad - \log_{10} \left[ \Gamma\left(\frac{d}{2} + 1\right) \right] - \frac{1}{2} \sum_j \log_{10} \omega_j. \end{aligned}$$

This lets us directly compute the log of tiny tail probabilities given the log of tiny  $x$  values, all the way down to the absurdly small value of  $\log_{10} F(x) = -\text{realmax} \approx -10^{308}$  (`realmax` is the largest double-precision number), i.e.  $F(x) = 10^{-10^{308}}$ , all in fast double precision.

We can also set lower and upper error bounds  $F_{\min}$  and  $F_{\max}$  for this cdf estimate, as the ellipse volume times the lowest and highest multinormal densities on the ellipse, i.e. at the points  $e_f$  and  $e_n$  on the ellipse that are farthest and nearest to the origin respectively. (The estimate is closer to the true value than this bound indicates, and even tighter bounds could be found, but this one is good enough as a first simple calculation.) These points are equidistant from the ellipse center on opposite sides of it, lying on the line from the origin to the ellipse center. So they are of the form  $c(1 \pm r)$ , and  $r$  is found by requiring that they satisfy the equation of the ellipse:

$$e_f, e_n = c(1 \pm r), \quad r = \sqrt{\frac{x}{\sum_j c_j^2 \omega_j}}.$$

Using these points we can express the bounds as fractions of

the estimate itself:

$$\begin{aligned} \frac{F_{\min}}{F} &= e^{(\|c\|^2 - \|e_f\|^2)/2} = e^{-\|c\|^2(r^2 + 2r)/2} \\ \Rightarrow \frac{\Delta F^-}{F} &= \frac{F - F_{\min}}{F} = 1 - e^{-\|c\|^2(r^2 + 2r)/2}, \\ \text{similarly } \frac{\Delta F^+}{F} &= \frac{F^{\max} - F}{F} = e^{-\|c\|^2(r^2 - 2r)/2} - 1. \end{aligned}$$

If these relative errors were constants, as we approach the tail end and the estimate goes to 0, the relative error would stay the same fraction of the estimate. But as  $x \rightarrow 0$ ,  $r \rightarrow 0$ , and these estimation errors, even as a fraction of the estimate, go to 0 and the estimate becomes exact.

We can simplify the expressions for the relative errors at the limit, using the Maclaurin series of  $r$  and taking only up to the linear term, which gives us symmetric error bounds:

$$\lim_{x \rightarrow 0} \frac{\Delta F^-}{F} = \lim_{x \rightarrow 0} \frac{\Delta F^+}{F} = \|c\|^2 r = \|c\|^2 \sqrt{\frac{x}{\sum_j c_j^2 \omega_j}}.$$

We can again take the log of this to be able to compute small relative error bounds using the log of tiny  $x$  values. We can also invert this relationship to decide where we can reliably use the ellipse approximation. If we want a relative error of no more than  $\delta$ , then we can use the approximation in the range  $x < \delta^2 / \|c\|^4 \sum_j c_j^2 \omega_j$ . For example, take  $w = [3 \ 1 \ 2]$ ,  $k = [4 \ 2 \ 3]$ ,  $\lambda = [7 \ 0 \ 2]$ ,  $s = m = 0$ . For a relative error of  $< 1\%$ , we can use the approximation for  $x < 3 \times 10^{-5}$ .

Fig. 2, left, compares the ellipse cdf estimate to Ruben's method for the above parameters, in the range where the computed cdf is around `realmin`, so Ruben's method falls to 0 at some point. We compute the log of the Ruben cdf for this plot, and log becomes an erroneous operation at such low values, so the Ruben curve zig-zags before disappearing. For the ellipse estimate we can directly compute the log, and continue much further down without any numerical issues. The error-band shows  $10^{35}$  times the error around the ellipse estimate, so the error is actually very tiny. The way we plotted these error-bands of  $F \pm \alpha \Delta F$  ( $\alpha = 10^{35}$ ) on a log axis is the following. Recall that the ellipse method returns the relative estimation error  $\delta$ . Then we can write:

$$\log_{10}(F \pm \alpha \Delta F) = \log_{10} F + \log_{10}(1 \pm \alpha \delta) \approx \log_{10} F \pm \frac{\alpha \delta}{\ln 10},$$

where in the second step we assume small  $\delta$ , and have taken up to the linear term of its Maclaurin series.

In summary, we can see that the ellipse method agrees very well with Ruben's method in this tail, and helps to extend it down to even smaller cdf values with tightening accuracy.

These results can be easily extended to the case of all-negative  $w_i$ , where the distribution is flipped and the upper tail is finite, and also when the offset is shifted to a non-zero  $m$ .

## 5.2 Computing the pdf

The ellipse approximation can also provide an expression for the pdf in the finite tail, by simply differentiating the cdf, eq. 2, w.r.t.  $x$ :

$$\lim_{x \rightarrow 0} f(x) = \frac{x^{\frac{d}{2}-1} d e^{-\frac{\|c\|^2}{2}}}{2^{\frac{d}{2}+1} \Gamma\left(\frac{d}{2} + 1\right) \sqrt{\prod_j \omega_j}}. \quad (3)$$

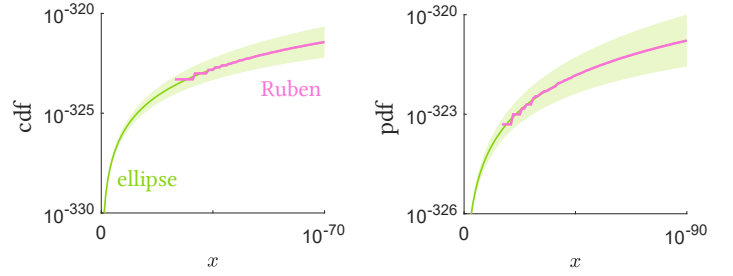


**Figure 2:** Comparing the ellipse approximation with Ruben's method for computing the cdf (left) and pdf (right) in the finite tail. Error-bands represent  $10^{35}$  times the error for the ellipse cdf estimate, and  $10^{45}$  times the error for the ellipse pdf estimate.

We can again take the log of this to be able to compute the log of tiny density values at tiny  $x$  values, down to  $f(x) = 10^{-10^{308}}$ . We can again set error bounds here, based on the closest and farthest points on the ellipse, which leads to the same relative error as for the cdf.

Fig. 2, right, compares the pdf computed by the ellipse method and Ruben's method (which is the best pdf method for the finite tail), for the same parameters again. The error-band here shows  $10^{45}$  times the error of the ellipse method, so it is again tiny. So for the pdf too, the ellipse method agrees well with Ruben's method and extends it much further into the tail.

## 6 Comparing the methods

### 6.1 Computing the cdf

In fig. 3a, we compute the cdf of a generalized chi-square with  $w = [2 \ 4 \ .5]$ ,  $k = [3 \ 5 \ 1]$ ,  $\lambda = [4 \ 1 \ .3]$ ,  $s = m = 0$ , which has a lower finite tail and an upper infinite tail. We use Imhof's method (with double precision for the middle and variable precision in the tails, and a relative error tolerance of  $10^{-10}$ ), IFFT (with a grid of  $N = 10^7$  points that spans a width of  $10^7$ ), ray-tracing. We use Ruben's method (with 100 terms) and the ellipse approximation only in the finite tail. To clearly show both the center and the tails of the distribution in the same plot, we have used a few plotting tricks. First, we plot the lower tail probability (cdf) until the median (cdf=0.5), and the upper tail probability (complementary cdf) beyond it, so that we can show both tails on the same log axes. Second, we select the main body of the distribution here to be the region above a lower or upper tail probability of 0.001 (area highlighted yellow). We use linear horizontal and vertical axes to show this area clearly, but in the tails we use log horizontal and vertical axes (areas highlighted red). Missing dots are where a method wrongly computes a small tail probability as 0, so it cannot be shown on a log axis.

We see that in the center of the distribution, all three methods agree well. In the finite lower tail, Imhof's method reaches accurately down to about  $10^{-6}$ , beyond which it returns incorrect values, sometimes negative, which we clip to 0, so those points are missing on this log plot (while discussing fig. 3b we shall elaborate on this limitation). The IFFT method with its settings here levels out at around  $10^{-5}$ , so it is not very accurate without sacrificing much more in terms of speed. The ray-trace method with

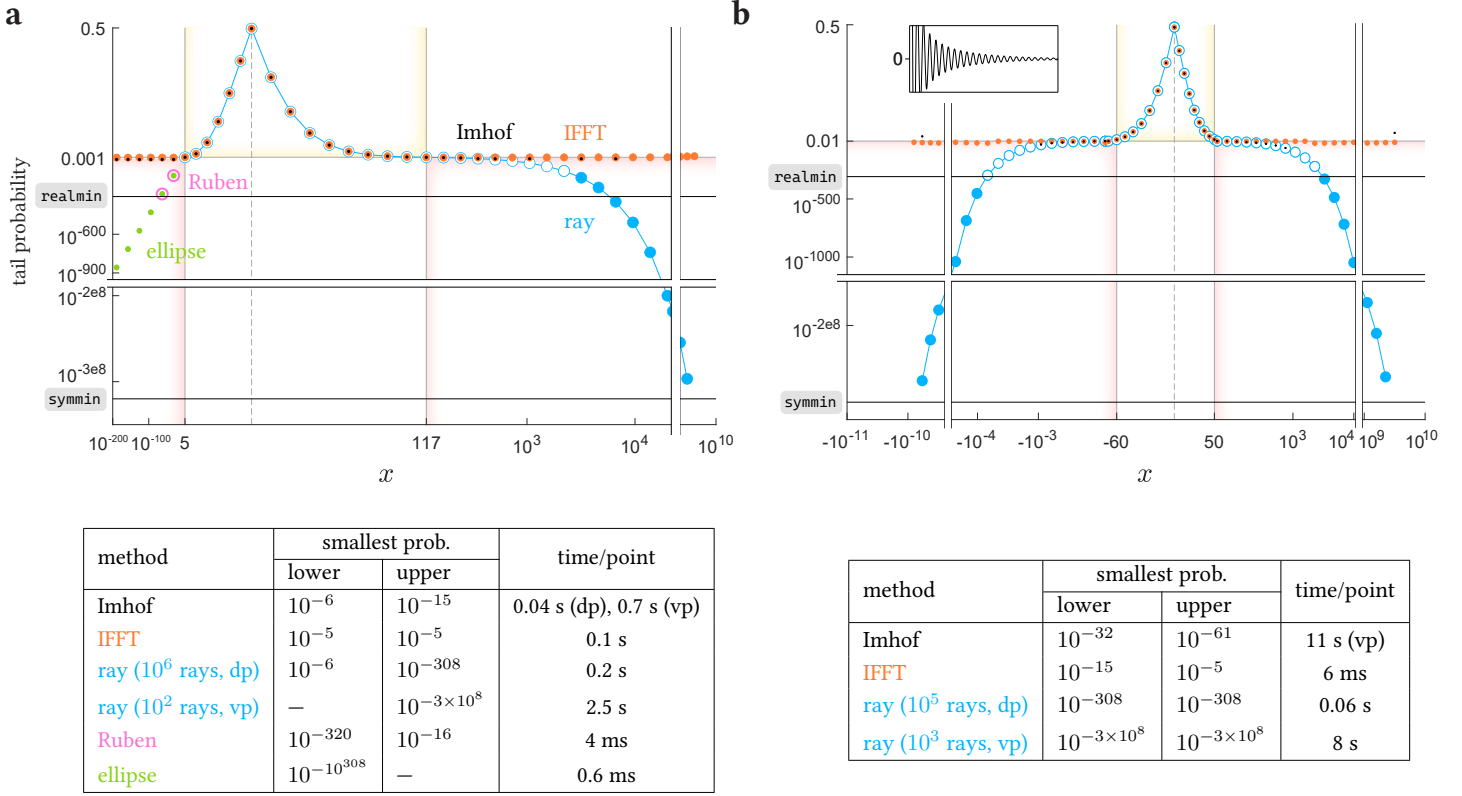


**Figure 3:** Computing the generalized chi-square cdf. **a.** Cdf of a generalized chi-square with a lower finite and upper infinite tail, computed with Imhof, IFFT, and ray-trace method with double precision (open circles) and variable precision (filled). We plot the lower tail probability (cdf) till the median (dashed vertical line), and upper tail probability (complementary cdf) beyond it. The middle of the distribution, probabilities  $>0.001$  (area highlighted yellow) is in linear axes, and the tail regions (areas highlighted red) are in double log axes. The vertical and horizontal white stripes are breaks in the axes, to be able to show the end of the upper tail in the bottom-right, which is much farther below. `realmin` =  $10^{-308}$  is the double-precision limit, and `symmin`  $\approx 10^{-3 \times 10^8}$  is the variable-precision limit. Any missing dots are where a method wrongly computes the tail probability as 0. The table below shows the orders of the smallest lower (finite) and upper (infinite) tail probabilities reached by the different methods with their respective settings, and their computation times per point. ‘dp’ and ‘vp’ mean double and variable precision. **b.** Cdf of a generalized chi-square with two infinite tails computed with the methods. Middle area of probability  $>0.01$  is in linear axes, tail areas are in log axes. Inset: Imhof integrand at  $x = -2000$ . Table below shows smallest lower and upper tail probabilities reached and computation times.

double precision stops at  $10^{-6}$  and returns 0 below that, due to the reason of the vanishing ellipsoidal integration domain we described in sec. 3.1. This limits the ray method in this finite tail well before `realmin`, and variable precision does not even kick in. Ruben’s method computes accurately down to about `realmin`, and the ellipse method can compute accurately all the way down to  $10^{-10^{308}}$ , which we don’t show here. In the infinite upper tail, Imhof’s method returns incorrect values below  $10^{-15}$ , even with variable precision, and IFFT again flattens out at  $10^{-5}$ . Here ray-trace with double precision continues for hundreds more orders of magnitude down to `realmin`, beyond which it uses variable precision to continue for *hundreds of millions* more orders of magnitude to `symmin`, which is so far down that we have breaks in the vertical and horizontal axes to show it in the same plot.

In the table below the figure, we list the smallest upper and lower tail probabilities that could be reached using these methods with these settings, along with the computation speeds on an 8-core 3.9GHz Intel Xeon W-2245 CPU. Ray-trace can also use an onboard NVIDIA GeForce RTX 3070 GPU (but only with double precision) and can be about 4 times faster than the CPU, but only when using at least about  $10^6$  rays, due to overhead. With vari-

able precision on the CPU, it takes the same time regardless of how small the output is, all the way down to `symmin`. All computation times reported henceforth are on this hardware.

In summary, all the exact methods are good for the middle of the distribution. Only Ruben and the ellipse approximation are good for the far lower finite tail. In the far upper infinite tail, ray-trace is the best.

We can also use our methods to compute the cdf of a non-central chi-square, which is a special case of the generalized chi-square, see supp. fig. S1. Matlab’s `ncx2cdf` implements a fast and relatively straightforward calculation for this special case, and can reach down to `realmin` in its finite lower tail, where the ray method again stops short due to the vanishing domain. But in the infinite upper tail, `ncx2cdf` stops at  $10^{-18}$ , whereas ray-trace reaches `realmin` with double precision and `symmin` with variable precision. In summary, for non-central chi-square cdf’s, `ncx2cdf` is the best method for the lower tail and center, but in the upper tail the ray method is best.

In fig. 3b we compute probabilities of a generalized chi-square with  $w = [1 \ -5 \ 2]$ ,  $k = [1 \ 2 \ 3]$ ,  $\lambda = [2 \ 3 \ 7]$ ,  $s = 10$  and  $m = 5$ , which has two infinite tails. We use Imhof’s method

$\tilde{\chi}$ type	part	best cdf method(s)	best pdf method(s)
$w_i$ same sign, $s = 0$	body	Ruben, Imhof, IFFT	Ruben, Imhof, IFFT
	finite tail	Ruben, ellipse	Ruben, ellipse
	infinite tail	ray	ray
$w_i$ mixed signs, and/or $s \neq 0$	body	Imhof, IFFT	Imhof, IFFT
	infinite tails	ray	ray

**Table 1:** The best cdf and pdf methods to use for the different parts of the distribution in different cases.

(with variable precision and relative error tolerance of  $10^{-15}$ ), the IFFT method (with a grid of  $N = 5 \times 10^5$  points spanning 100 times the input range), and the ray-trace method (using  $10^5$  rays with fast double-precision in the middle, and  $10^3$  rays with slow variable-precision in the tails). In the center of the distribution the methods again agree well. But in the tails, the Imhof method again computes small probabilities inaccurately, and they are often negative (which we clip to 0 and these are the missing black dots). This is because in the tail, the Imhof integrand related to the characteristic function (see inset) is highly oscillatory and integrates to a tiny probability. So when numerically integrated, the larger oscillations must be computed to precisely cancel and accurately produce the tiny residual sum. When this does not work so precisely, the integral is either above or below the true value. The ray method is an entirely different approach where the contribution to the integral from each ray is non-negative, and they never cancel each other. So it avoids this problem and can again reach down to `realmin` quite fast with double precision, and then to `symmin` with variable precision, while still matching Imhof in speed. It works well in both tails here because they are both infinite. The IFFT method is extremely fast, but less capable of accurately reaching such small tail probabilities. The table below the figure lists the smallest tail probabilities that could be reached by these methods with these settings, along with their speeds.

Our `gx2inv` function uses root-finding on a cdf function to compute the inverse cdf. Since the ray method can compute such small probabilities in an infinite tail, `gx2inv` can leverage this to find quantiles corresponding to probabilities in an infinite tail that are as small as `symmin`, which is not possible by inverting other cdf methods.

## 6.2 Computing the pdf

Fig. 4c shows a comparison of the Imhof, IFFT and ray methods to compute a generalized chi-square pdf. Imhof may take a lot more time here than for the cdf because the lack of  $1/u$  in the integrand makes it converge slower.

## 7 More accuracy tests

### 7.1 Against published tables

Imhof<sup>22</sup> provides a table that lists some upper tail cdf values of some generalized chi-square distributions with mixed-sign weights (but with  $s = m = 0$ ). In table 2, nos. 1-12, we list those ‘exact’ values. No information is provided about their accuracy, so we assume that they are rounded to four places, i.e.

their uncertainty is  $\pm 0.5$  in the last digit. Liu et al<sup>26</sup> also provide a table that lists some upper tail cdf values of some generalized chi-square distributions with only positive weights (i.e. these are all infinite tails), computed with Ruben’s exact method to a greater precision of 6 digits (nos. 13-16 here). We compare the outputs from our implementations of Imhof, ray-trace and IFFT methods against these exact values, using roughly the minimum settings needed to reach this precision.

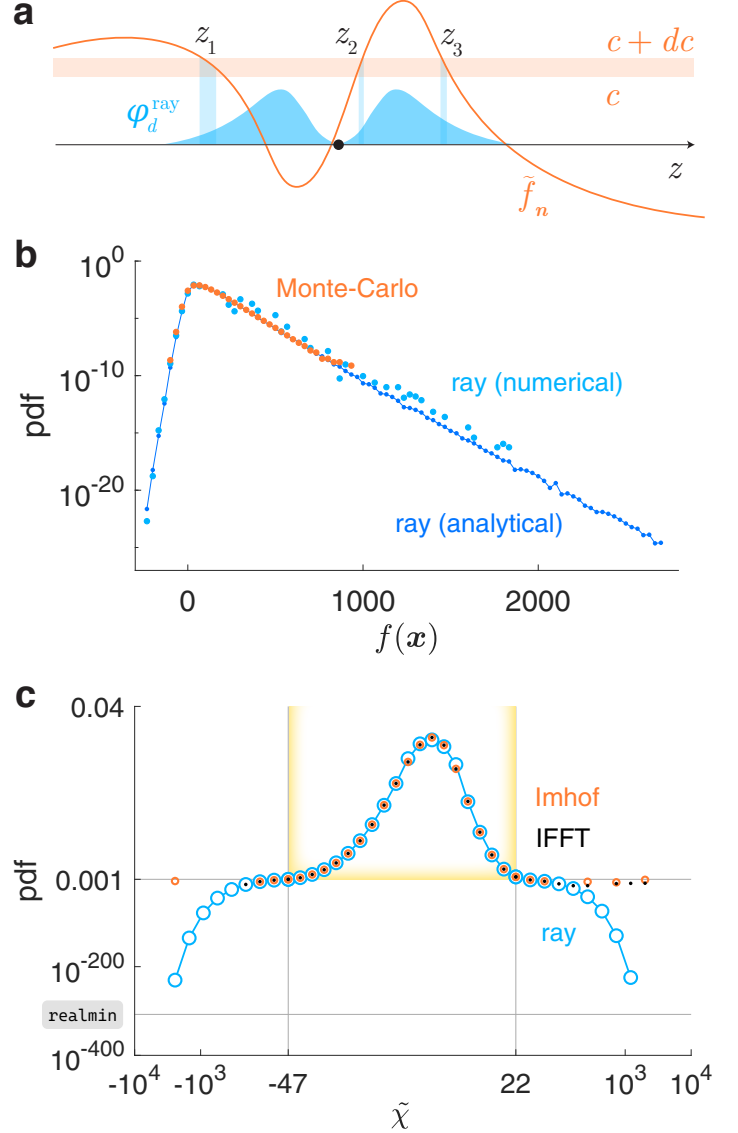


**Figure 4:** Computing the pdf. **a.** The ray-tracing method to compute the pdf of a function  $f(\mathbf{x})$  of a normal vector  $\mathbf{x}$ . The arrow is a ray through the mean (dot) of a standard multinormal along  $\mathbf{n}$ , and the blue pdf  $\phi_d^{\text{ray}}$  is the standard multinormal density along the ray.  $\tilde{f}_n(z)$  is the value of the standardized function  $\tilde{f}(z)$  along the ray. The intervals where  $\tilde{f}_n$  lies between  $c$  and  $c+dc$  are the blue widths at  $z_1, z_2$  and  $z_3$ . **b.** The pdf of a cubic function of a 4d normal vector, computed by Monte-Carlo sampling, vs. numerically differentiating the ray method cdf, vs. using the analytical derivative. Missing dots are where a method wrongly computes the pdf as 0. **c.** A generalized chi-square pdf computed with Imhof’s method, IFFT of the characteristic function, and ray method. Middle highlighted area (density  $> 0.001$ ) is in linear axes, log axes outside.



#	$\tilde{\chi}$ parameters	$x$	exact value	Imhof		ray-trace		IFFT	
				value	time	value	time	value	time
1	$w = [.6 \ .3 \ .1]$ $k = [1 \ 1 \ 1]$ $\lambda = [0 \ 0 \ 0]$	.1	.9458	.9458(1)	0.04 s	.9458(1)	3.5 s (GPU, MC w $10^7$ rays)	.9458	0.1 s (span = $10^4$ , $N = 10^6$ )
		.7	.5064	.5064(1)		.5064(1)		.5064	
		2	.1240	.1240(1)		.1240(1)		.1240	
2	$w = [.6 \ .3 \ .1]$ $k = [2 \ 2 \ 2]$ $\lambda = [0 \ 0 \ 0]$	.2	.9936	.993547(1)	0.03 s	.993545(5)	3.5 s (GPU, MC w $10^7$ rays)	.993546	9.5 s (span = $10^6$ , $N = 10^8$ )
		2	.3998	.399795(1)		.3997(1)		.3998	
		6	.0161	.016103(1)		.01610(1)		.0161	
3	$w = [.6 \ .3 \ .1]$ $k = [6 \ 4 \ 2]$ $\lambda = [0 \ 0 \ 0]$	1	.9973	.9973(1)	0.01 s	.997319(3)	4.7 s (GPU, MC w $10^7$ rays)	.9973	0.1 s (span = $10^5$ , $N = 10^6$ )
		5	.4353	.4353(1)		.4353(1)		.4353	
		12	.0088	.0088(1)		.008770(7)		.0088	
4	$w = [.6 \ .3 \ .1]$ $k = [2 \ 4 \ 6]$ $\lambda = [0 \ 0 \ 0]$	1	.9666	.9666(1)	8 ms	.96665(3)	4.8 s (GPU, MC w $10^7$ rays)	.9666	0.08 s (span = $10^5$ , $N = 10^6$ )
		3	.4196	.4196(1)		.4196(1)		.4196	
		8	.0087	.00871(1)		.00871(1)		.0087	
5	$w = [.7 \ .3]$ $k = [6 \ 2]$ $\lambda = [6 \ 2]$	2	.9939	.9939(1)	7 ms	.99391(9)	1 s (GPU, MC w $10^6$ rays)	.9939	1 s (span = $10^6$ , $N = 10^7$ )
		10	.4087	.4087(1)		.4087(2)		.4087	
		20	.0221	.0221(1)		.02210(6)		.0221	
6	$w = [.7 \ .3]$ $k = [1 \ 1]$ $\lambda = [6 \ 2]$	1	.9549	.9549(1)	0.01 s	.9548(1)	0.1 s (grid integral)	.9549	1 s (span = $10^6$ , $N = 10^7$ )
		6	.4076	.4076(1)		.4076(1)		.4076	
		15	.0223	.0223(1)		.0223(1)		.0223	
7	$w = [.2 \ .1 \ .\frac{1}{3} \ .4 \ .\frac{2}{3}]$ $k = [10 \ 4 \ 2 \ 2 \ 6]$ $\lambda = [0 \ 0 \ 0 \ 0 \ 0]$	1.5	.9891	.9891(1)	0.01 s	.98906(1)	8.4 s (GPU, MC w $10^7$ rays)	.9891	2.5 s (span = $2 \times 10^5$ , $N = 2 \times 10^7$ )
		4	.3453	.3453(1)		.3453(1)		.3453	
		7	.0154	.0154(1)		.01541(2)		.0154	
8	$w = [.2 \ .1 \ .\frac{1}{3} \ .4 \ -.2 \ -.2]$ $k = [6 \ 4 \ 2 \ 2 \ 4 \ 6]$ $\lambda = [0 \ 0 \ 0 \ 0 \ 0 \ 0]$	-2	.9102	.910225(1)	.01 s	.91024(4)	2.8 m (GPU, MC w $2 \times 10^8$ rays)	.9102	14 s (span = $10^6$ , $N = 10^8$ )
		0	.4061	.406106(1)		.40609(9)		.4061	
		2.5	.0097	.009760(1)		.009758(7)		.00976	
9	$w = [\frac{7}{2} \ .\frac{3}{2}]$ $k = [7 \ 3]$ $\lambda = [12 \ 4]$	3.5	.9563	.9563(1)	7 ms	.9564(2)	0.7 s (GPU, MC w $10^6$ rays)	.9563	9.5 s (span = $10^6$ , $N = 10^8$ )
		8	.4152	.4152(1)		.4152(1)		.4152	
		13	.0462	.0462(1)		.0463(1)		.0462	
10	$w = [\frac{7}{2} \ .\frac{3}{2} \ -.7 \ -.3]$ $k = [6 \ 2 \ 1 \ 1]$ $\lambda = [6 \ 2 \ 6 \ 2]$	3.5	.9218	.9218(1)	9 ms	.9215(3)	0.8 s (GPU, MC w $10^6$ rays)	.9218	1.2 s (span = $10^6$ , $N = 10^7$ )
		8	.4779	.4779(1)		.4780(2)		.4779	
		13	.0396	.0396(1)		.0397(1)		.0396	
11	$w = [\frac{6}{4} \ .\frac{3}{4} \ .\frac{1}{4} \ .7 \ .4]$ $k = [8 \ 11 \ 8 \ 7]$ $\lambda = [0 \ 4 \ 0 \ 12]$	3	.9842	.9842(1)	6 ms	.9842(1)	1.1 s (GPU, MC w $10^6$ rays)	.9842	1.3 s (span = $10^6$ , $N = 10^7$ )
		6	.4264	.4264(1)		.4263(3)		.4264	
		10	.0117	.0117(1)		.01165(6)		.0117	
12	$w = [.1 \ .\frac{1}{2} \ .\frac{1}{6} \ -.7 \ -.1 \ .\frac{7}{3} \ -.2 \ -.1 \ -.1]$ $k = [7 \ 4 \ 2 \ 6 \ 2 \ 1 \ 2 \ 4 \ 6]$ $\lambda = [2 \ 0 \ 0 \ 6 \ 2 \ 6 \ 0 \ 0 \ 0]$	-3	.9861	.9861(1)	8 ms	.9862(1)	1.1 s (GPU, MC w $10^6$ rays)	.9861	0.1 s (span = $10^5$ , $N = 10^6$ )
		0	.5170	.5170(1)		.5170(5)		.5170	
		4	.0152	.0152(1)		.0152(1)		.0152	
13	$w = [.5 \ .4 \ .1]$ $k = [1 \ 2 \ 1]$ $\lambda = [1 \ .6 \ .8]$	2	.457461(1)	.457461(1)	0.02 s	.457461(1)	2.5 s (grid integral)	.457460	33 s (span = $4 \times 10^6$ , $N = 2 \times 10^8$ )
		6	.031109(1)	.031109(1)		.031109(1)		.031109	
		8	.006885(1)	.006885(1)		.006885(1)		.006886	
14	$w = [.7 \ .3]$ $k = [1 \ 1]$ $\lambda = [6 \ 2]$	1	.954873(1)	.954873(1)	0.09 s	.954873(1)	0.3 s (grid integral)	.954872	31 s (span = $4 \times 10^6$ , $N = 2 \times 10^8$ )
		6	.407565(1)	.407565(1)		.407565(1)		.407565	
		15	.022343(1)	.022343(1)		.022343(1)		.022344	
15	$w = [.995 \ .005]$ $k = [1 \ 2]$ $\lambda = [1 \ 1]$	2	.347939(1)	.347939(1)	0.2 s	.347939(1)	0.4 s (grid integral)	.347938	1.3 m (span = $4 \times 10^6$ , $N = 10^9$ )
		8	.033475(1)	.033475(1)		.033475(1)		.033476	
		12	.006748(1)	.006748(1)		.006748(1)		.006749	
16	$w = [.35 \ .15 \ .35 \ .15]$ $k = [1 \ 1 \ 6 \ 2]$ $\lambda = [6 \ 2 \ 6 \ 2]$	3.5	.956318(1)	.956318(1)	7 ms	.956322(8)	7 m (GPU, MC w $10^9$ rays)	.956318	2.8 m (span = $10^7$ , $N = 10^9$ )
		8	.415239(1)	.415239(1)		.415234(5)		.415239	
		13	.046231(1)	.046231(1)		.046230(4)		.046231	

**Table 2:** Testing the accuracy of computing the generalized chi-square upper-tail cdf (probability that  $\tilde{\chi}$  exceeds  $x$ ) with our implementations of Imhof, ray-trace and IFFT methods, against previously published exact values in Imhof’s table<sup>22</sup> (nos. 1-12, which have mixed-sign weights, and which we assume are rounded to 4 places, i.e. have an uncertainty of  $\pm 0.5$  in the last digit), and Liu et al’s table<sup>26</sup> (nos. 13-16, which have all positive weights, computed with Ruben’s method<sup>21</sup> to 6 digits). In all cases, the parameters  $s = m = 0$ . Digits in parentheses at the end signify uncertainty, eg (1) means  $\pm 1$  in the last digit. IFFT does not return uncertainty, and its values are rounded to the last digit. In each row, all green values match each other within uncertainty. Our methods are used with roughly the minimum settings needed to reach the required precision. Reported times are to compute all three cdf values of a distribution. ‘MC’ means Monte-Carlo integration.

Up to 4 total degrees of freedom, the ray method can be used with adaptive grid integral, to the error tolerance that we specify. Beyond this it performs slower Monte-Carlo integration (on the GPU here), and reports the standard error of the output, and we increase the number of Monte-Carlo rays (mentioned in the table) until we reach the required precision. The IFFT method does not report uncertainty values, but we increase its grid span and number of grid points  $N$  (mentioned in the table) until its output converges to the desired precision.

We see that in almost all cases, all our values match each other and the exact values within uncertainty. (If two numbers are  $p_1 \pm \Delta p_1$  and  $p_2 \pm \Delta p_2$ , they agree if  $|p_1 - p_2| \leq \Delta p_1 + \Delta p_2$ .) In two cases, Imhof’s published exact values deviate slightly from the uncertainty range of our values (including our implementation of Imhof’s method itself), and we believe that our values are more correct, since we compute them to greater precision and they match each other.

Unlike the case of fig. 3, say, Imhof’s method is by far the

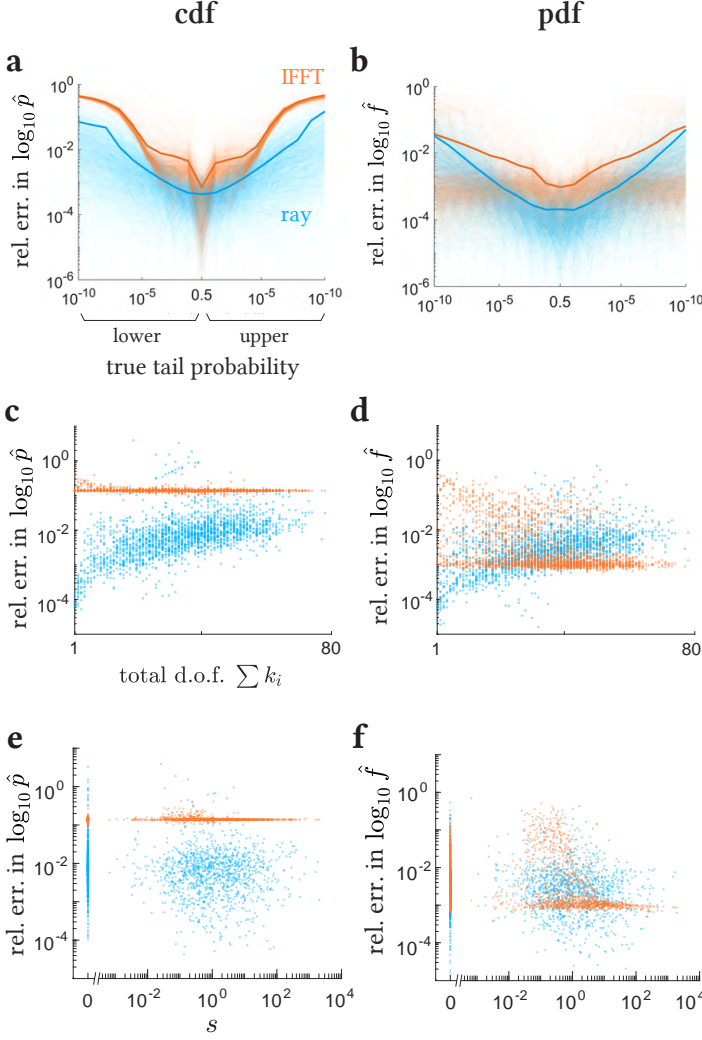


**Figure 5:** Relative errors in estimating the cdf (left column of plots) and pdf (right column of plots) of 2000 randomly sampled generalized chi-square distributions, by the IFFT and ray methods, with respect to Imhof method estimates as the ground truth. **a:** Relative error in estimating the order of the lower or upper tail cdf, against an array of quantile points. Faint lines are all 2000 distributions, thick lines are the average. **b:** Similar plot for estimating the pdf at those points. **c:** Relative error of cdf estimates against the total degrees of freedom of each distribution. **d:** Similar plot for pdf estimates. **e:** Relative error of cdf estimates against the value of  $s$  of each distribution. **f:** Similar plot for pdf estimates.

fastest here for the same accuracy, and therefore the best. This is for two reasons. First, here we compute values over only three points, whereas ray-trace and IFFT use vector operations that are faster when simultaneously computing values over many points. Second, these values were not too far in the tails and only had up to 6 decimal places, but when we are far in the tails or need much more accuracy, the Imhof integral slows down or quits with a wrong value, compared to ray-trace.

## 7.2 With randomly sampled parameters

Bodenham et al<sup>29</sup> have suggested that testing the accuracy of methods on a few points across some hand-picked distributions, as in the previous section, is not thorough enough, and instead

recommend to randomly sample a large set of generalized chi-square parameters, then compare the methods across an array of quantile points for each distribution in the set. In this section we show performance tests along these lines.

We first randomly sample a broad set of parameters. We draw the number  $n$  of constituent non-central chi-square terms uniformly from 1 through 10. Then we draw each of the  $n$  weights  $w_i$  from a standard normal distribution, and each of the  $n$  degrees of freedom  $k_i$  uniformly from 1 through 10. Each non-centrality  $\lambda_i$  is with equal probability either 0 (so that term is a central chi-square), or equal to  $10^z$ , where  $z$  is a standard normal, so that the non-centrality can spread across several orders of magnitude. Similarly,  $s$  is with equal probability either 0 (so that there is no linear term), or equal to 10 raised to a standard normal.  $m$  is also drawn similarly to  $s$ , except that its sign is positive or negative with equal probability.

Now we select an array of 10 lower tail probability (cdf) values, uniformly logarithmically spaced from  $10^{-10}$  to 0.5 (the median), then upper tail probability (complementary cdf) values similarly arrayed from the median to  $10^{-10}$ . Now, for each distribution in our list, we use our `gx2inv` function to find the 19 quantiles corresponding to these probabilities. `gx2inv` may not always compute very accurate quantile values, but this does not matter for our accuracy test here.

At each of these quantiles, we first compute the tail probability, and the probability density, using the Imhof method with variable precision and a small relative error tolerance of  $10^{-15}$ , so that we have reliable ground-truth values. We then compute those cdf and pdf values using the ray method (with double precision, and  $2 \times 10^6$  rays for the cdf and  $10^7$  rays for the pdf), and IFFT (with a span of  $10^5$  times the range from the lowest to the highest quantile, and  $2 \times 10^7$  grid points for the cdf, and a span of  $4 \times 10^5$  times that range, and  $10^8$  grid points for the pdf). These settings were selected roughly with trial and error on a couple of distributions, and are not sacrosanct, and with these settings ray and IFFT need roughly equal time. For computing all 19 cdf values for each distribution, ray took an avg.  $\pm$  sd of  $5.9 \pm 1.3$  s, and IFFT took  $5.3 \pm 1.2$  s. For computing all the pdf values for each distribution, ray took  $13.1 \pm 2.3$  s, and IFFT took  $15.4 \pm 2.9$  s.

We ran this test across across 2000 randomly sampled distribution parameters. At each quantile for each distribution, we compute the relative error in estimating the log probability:  $|(\log_{10} \hat{p} - \log_{10} p) / \log_{10} p|$ , where  $p$  is the tail probability (cdf below median, and complementary cdf above median) computed by the Imhof method, and  $\hat{p}$  by ray or IFFT. We measure the error in estimating  $\log_{10} p$  instead of  $p$ , because  $p$  is arrayed across several scales, and we find that the estimation errors of its order of magnitude, and not the value itself, are what is more comparable across these different scales. At each of these points we also similarly compute the relative error in estimating the log probability density.

Across all 19 quantiles of all 2000 distributions, the average relative error of estimating the log tail probability was 0.02 by the ray method, and 0.14 by the IFFT method, so the ray method was considerably better for the same computation time. The average relative errors of estimating the log probability densities were smaller for both, 0.008 for ray and 0.015 for IFFT, so ray was again better for the same time.

Now we look at the variation in performance across different parameters. Figs. 5a and b show the relative estimation errors in cdf and pdf across the different quantile values. We see that with both methods, the errors climb as we go out to the tails, and overall the ray method is better. For cdf estimation the ray method has more variance in performance, whereas the IFFT method is tighter in its error, particularly in the tails.

Fig. 5c shows the average relative estimation error of the cdf across all quantiles, as a function of the total degrees of freedom of each distribution. We see that the ray method is overall better, but its error climbs with the total d.o.f. This makes sense since this is the number of dimensions of the space in which it is integrating, so a fixed number of rays would be sampling the space more sparsely as the dimension grows, and will miss more features of the integration domain. The error of the IFFT is higher, but more static across d.o.f, since it is always computing a one-dimensional integral of the characteristic function, regardless of the total d.o.f. Fig. 5d shows similar results for computing the pdf, but now the IFFT method is relatively better, and in fact shows slight improvement with increasing d.o.f.

Figs. 5e and f show the performance variation as a function of the linear  $s$  term. We see that in general, the value of  $s$ , whether 0 or across different scales, has little effect on the performance of the methods, although the IFFT method improves slightly with higher  $s$ , as particularly visible for the pdf. This could be because the factor of  $e^{-s^2 t^2/2}$  in the characteristic function  $\phi(t)$  suppresses its tails and shrinks its width, so it is captured better by an inverse Fourier transform with the same grid span and density.

$m$  is just an offset and we have checked that it has no bearing on performance of either of the methods, so we don't plot it here.

In summary, we see that across a wide sample of distributions, the ray method is overall better than IFFT for computing the cdf, but for the pdf they are more similar on average, and the ray method has more overall variance in performance.

### 7.3 With equal-covariance multinormals

The ray method in particular extends farthest into the tails than any other method, while agreeing well with existing exact methods in the center of the distributions. But are those far tail probabilities and densities computed by the ray method correct? From the tests we have used so far, we cannot say. It is difficult to directly check the ray method against any other exact method so far in the tails, since no other method can compute accurately there in reasonable time. So here we show an accuracy test of the ray-trace method in the far tail, with a special case where the ground-truth value is a manageable number, not too tiny or too large for machine representation, and which can be exactly and quickly calculated: the discriminability index  $d'$ .

$d'$  is a measure of statistical separation between two distributions, and for two multinormals with equal covariance  $\Sigma$ , it is given by the easily-calculable Mahalanobis distance between them:  $d' = \sqrt{(\mu_a - \mu_b)' \Sigma^{-1} (\mu_a - \mu_b)}$ . In a previous paper,<sup>7</sup> we had introduced the Bayes discriminability index  $d'_b = -2Z(p_e)$  that can be calculated from the classification error rate  $p_e$  of any two distributions in general, i.e. by computing the probability of each distribution on the wrong side of the classification

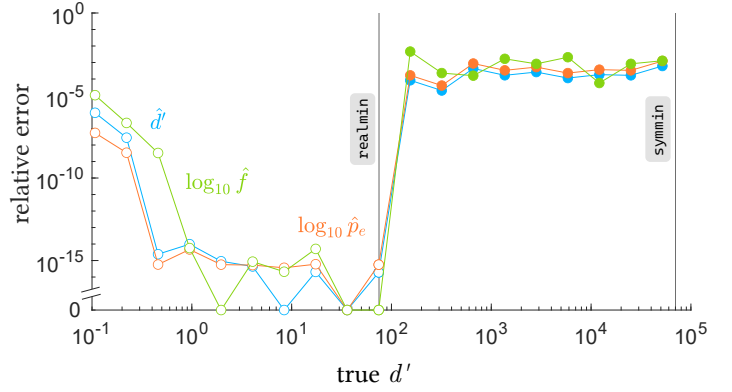


**Figure 6:** Relative inaccuracies in the ray method's estimates of the discriminability index  $\hat{d}'$  and order of magnitude of the classification error rate  $\hat{p}_e$  between two multinormals, and the order of magnitude of the probability density  $\hat{f}$  at the classification boundary, as we increase the true  $d'$  between the multinormals. Open and filled circles are for double precision and variable precision computations respectively. Vertical lines are the limits of computation in double precision (corresponding to an error rate of `realmin`) and variable precision (error rate of `symmin`).

boundary. For two equal-covariance multinormals, the classification boundary is a plane between them, and we can use the ray-tracing method to integrate the multinormals on either side of the boundary, and compute the error rate and the corresponding  $d'_b$ . In this equal-covariance case,  $d'_b$  should equal the Mahalanobis distance  $d'$ , so we can use this to test the accuracy of the ray method as we separate the two multinormals far apart, which takes us into the tail. Even though the equal-covariance is a simple case, ray-tracing still uses its full algorithm here, so this is a test for the entire general method.

We take two trivariate normals with the following covariance matrix:

$$\Sigma = \begin{bmatrix} 1 & .5 & .7 \\ .5 & 2 & 1 \\ .7 & 1 & 3 \end{bmatrix}$$

The first one stays at the origin while we move the mean of the second in logarithmic steps from the origin along the  $[1 \ 1 \ 1]$  vector. At each step we compute the true  $d'$  using the Mahalanobis distance, and we use the ray method to compute the classification error rate  $\hat{p}_e$  between the multinormals, and the Bayes discriminability index  $\hat{d}'$  from it. Fig. 6 shows the relative inaccuracy in this estimate  $\frac{|\hat{d}' - d'|}{d'}$  with increasing distance. We first use the ray method with grid integration in double precision (with a relative tolerance of  $10^{-20}$ ) to compute  $\hat{p}_e$  down to the double-precision limit `realmin`, which corresponds to  $\hat{d}' \approx 75$ , already a rarely high value. For small  $d'$  ( $<1$ ), the estimate is slower to converge to an accurate value, but for large values, which are more relevant when measuring the performance of good classifiers such as ideal observers, the ray method is quite accurate with an error of only around  $10^{-15}$ . In our previous paper,<sup>7</sup> fig. 7a, we had reported this accuracy up to the double-precision limit of  $d' \approx 75$ , but now we extend past it with variable precision, using Monte-Carlo integration with  $10^3$  rays, which yields a stable relative error of only around 0.01% all the way up to a ridiculously large  $d' \approx 70,000$  (an error rate of the variable-precision limit `symmin`), beyond which symbolic computation fails.



We can also directly test the accuracy in the ray method's estimate  $\hat{p}_e$  of the classification error rate itself, which is essentially a tail cdf, by comparing it to the true known error rate  $p_e = \bar{\Phi}(d'/2)$ . We noticed here that in the far tail, where the true  $p_e$  was of the order of  $10^{-145643038}$  at a point, the estimated  $\hat{p}_e$  was around  $10^{-145821748}$ . So in absolute terms,  $\hat{p}_e$  was only  $10^{-178710}$  of the true  $p_e$  and egregiously wrong, and the estimation error would be 100%. But arguably when comparing such tiny numbers, it is fairer to compare their orders of magnitude instead, which is off by only about 0.1% here. We also notice that similar to our random-sample tests, it is the relative error in the log of the probability or density that is more comparable across scales. So in fig. 6 we show the relative error in the estimate of the order of magnitude of  $p_e$ , i.e.  $|(\log_{10} \hat{p}_e - \log_{10} p_e) / \log_{10} p_e|$ , and we see that it closely follows the small estimation errors of the  $d'$ , which makes sense since  $d'$  and  $p_e$  are monotonic functions of each other.

We can also test the accuracy of computing the pdf by the ray method here, by computing the probability density of either of the multinormals at the planar classification boundary, which is the same as the density of a standard multinormal at a distance  $d'/2$ . The ray method is designed to compute the pdf of a *function* of a multinormal though, not the multinormal itself, but we can work around that easily. We take the trivariate standard normal in  $(x_1, x_2, x_3)$ , and at each step of  $d'$ , we use the ray method to compute the pdf of the 'function'  $g(x) = x_1$  at  $g = d'/2$  (again using grid integration with a relative tolerance of  $10^{-20}$  in double precision, and Monte-Carlo integration with  $10^3$  rays in variable precision). We can compare this density  $\hat{f}$  to the known true value of the density at the boundary,  $f = \phi(d'/2)$ . Like the cdf, this pdf is also tiny in the far tail, so we again look at the estimation error of its order of magnitude:  $|(\log_{10} \hat{f} - \log_{10} f) / \log_{10} f|$ . We see that the accuracy is comparable to those of  $\hat{d}'$  and  $\log_{10} \hat{p}_e$ .

To compute the tail probability  $\hat{p}_e$  and  $\hat{d}'$ , with grid integration in double precision it takes from 1 sec (large  $d'$ ) to 1 min (small  $d'$ ) per point, whereas Monte-Carlo integration with  $10^3$  rays in variable precision takes about 2 min per point. Computing the probability density  $\hat{f}$  with grid integration in double precision takes from 2 sec (large  $d'$ ) to 16 sec (small  $d'$ ) per point, whereas Monte-Carlo integration with  $10^3$  rays in variable precision takes a long 35 min per point, since the symbolic calculations for the pdf are slower.

## 8 Conclusion

In this paper we derived the mapping from generalized chi-square parameters to the parameters of the corresponding quadratic form of a multinormal, and presented two exact (IFFT and ray-trace) methods to compute the cdf and pdf of the distribution, and one approximate method (ellipse) which becomes exact in the limit of the finite tail. These methods are all accompanied by our open-source Matlab software. We compared the performance of these methods in terms of their agreement with each other, how far into the tail they can reach, their accuracy, and speed, and presented a table of the best methods to use in different cases. We also showed how the high-accuracy ray method can be used to measure large discriminability indices  $d'$  between two multinor-

mal distributions.

## 9 Acknowledgements

We thank Dr Luis Mendo Tomás (Universidad Politécnica de Madrid) and Dr Andrew D. Horchler (Astrobotic) for their generous help with my Stack Overflow questions on variable precision, and my longtime friend Dr Stefan Eccles (Okinawa Institute of Science and Technology) for backing up my multivariable calculus.

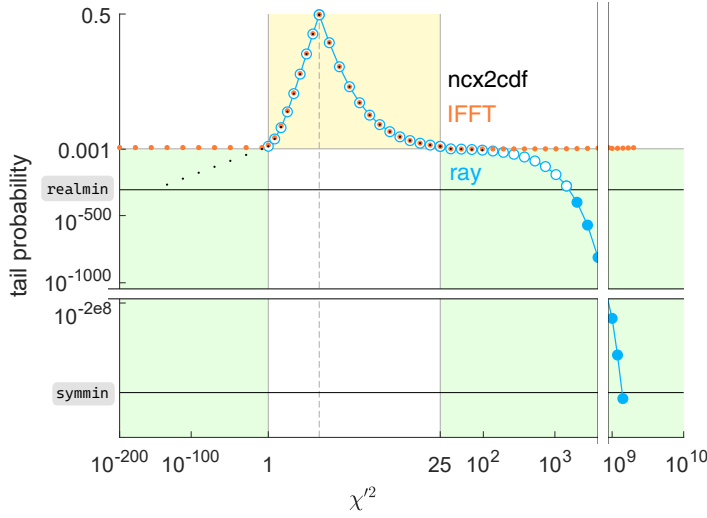
## References

- 1 DA Jones. Statistical analysis of empirical models fitted by optimization. *Biometrika*, 70(1):67–88, 1983.
- 2 Hayato Nishi and Ikuho Yamada. Counter-intuitive effect of null hypothesis on moran's i tests under heterogenous populations (short paper). In *12th International Conference on Geographic Information Science (GIScience 2023)*. Schloss Dagstuhl-Leibniz-Zentrum für Informatik, 2023.
- 3 Housen Li and Frank Werner. Adaptive minimax optimality in statistical inverse problems via solit-sharp optimal lepskii-inspired tuning. *arXiv preprint arXiv:2304.10356*, 2023.
- 4 Nisar Ahmed, Luke Burks, Kailah Cabral, and Alyssa Bekai Rose. Exact consistency tests for gaussian mixture filters using normalized deviation squared statistics. *arXiv preprint arXiv:2312.17420*, 2023.
- 5 Chowdhury Mohammad Rakin Haider, Chris Clifton, and Yan Zhou. Unfair ai: It isn't just biased data. In *2022 IEEE International Conference on Data Mining (ICDM)*, pages 957–962. IEEE, 2022.
- 6 Chun Yui Wong, Pranay Seshadri, Andrew B Duncan, Ashley Scillitoe, and Geoffrey Parks. Prior-informed uncertainty modelling with bayesian polynomial approximations. *arXiv preprint arXiv:2203.03508*, 2022.
- 7 Abhranil Das and Wilson S Geisler. Methods to integrate multinormals and compute classification measures. *arXiv preprint arXiv:2012.14331*, 2020.
- 8 Jeffrey S Hazboun, Patrick M Meyers, Joseph D Romano, Xavier Siemens, and Anne M Archibald. Analytic distribution of the optimal cross-correlation statistic for stochastic gravitational-wave-background searches using pulsar timing arrays. *arXiv preprint arXiv:2305.01116*, 2023.
- 9 Bruce Allen and Joseph D Romano. Hellings and downs correlation of an arbitrary set of pulsars. *Physical Review D*, 108(4):043026, 2023.
- 10 Stephan Weiss, Connor Delaosa, James Matthews, Ian K Proudler, and Ben A Jackson. Detection of weak transient signals using a broadband subspace approach. In *2021 Sensor Signal Processing for Defence Conference (SSPD)*, pages 1–5. IEEE, 2021.



- 11 Yao-Wen Hsu. Statistical model for approximating gains of arrays with unequal normally distributed errors. *IEEE Transactions on Antennas and Propagation*, 70(12):11653–11664, 2022.
- 12 Andrew Graff and Todd E Humphreys. Purposeful co-design of ofdm signals for ranging and communications. *arXiv preprint arXiv:2309.03076*, 2023.
- 13 Fabian Rothmaier, Yu-Hsuan Chen, Sherman Lo, and Todd Walter. A framework for gnss spoofing detection through combinations of metrics. *IEEE Transactions on Aerospace and Electronic Systems*, 57(6):3633–3647, 2021.
- 14 Birendra Kujur, Samer Khanafseh, and Boris Pervan. Optimal ins monitor for gnss spoofer tracking error detection. *NAVIGATION: Journal of the Institute of Navigation*, 71(1), 2024.
- 15 Paolo Manfredi. Probabilistic uncertainty quantification of microwave circuits using gaussian processes. *IEEE Transactions on Microwave Theory and Techniques*, 2022.
- 16 Hanxiao Liu, Yuqing Ni, Xiaofan Wang, and Lihua Xie. Linear attacks against remote state estimation: Performance analysis under an encryption scheme. *IEEE Transactions on Control of Network Systems*, 2024.
- 17 Kristoffer M Frey. *Belief-Space Planning for Real-World Systems: Efficient SLAM-Based Belief Propagation and Continuous-Time Safety*. PhD thesis, Massachusetts Institute of Technology, 2021.
- 18 Tyler Toner, Dawn M Tilbury, and Kira Barton. Probabilistically safe mobile manipulation in an unmodeled environment with automated feedback tuning. In *2022 American Control Conference (ACC)*, pages 1214–1221. IEEE, 2022.
- 19 Spencer Van Koevering, Yiwei Lyu, Wenhao Luo, and John Dolan. Provable probabilistic safety and feasibility-assured control for autonomous vehicles using exponential control barrier functions. In *2022 IEEE Intelligent Vehicles Symposium (IV)*, pages 952–957. IEEE, 2022.
- 20 Sooyung Byeon, Joonwon Choi, Yutong Zhang, and Inseok Hwang. Stochastic-skill-level-based shared control for human training in urban air mobility scenario. *ACM Transactions on Human-Robot Interaction*, 2023.
- 21 Harold Ruben. Probability content of regions under spherical normal distributions, iv: The distribution of homogeneous and non-homogeneous quadratic functions of normal variables. *The Annals of Mathematical Statistics*, 33(2):542–570, 1962.
- 22 Jean-Pierre Imhof. Computing the distribution of quadratic forms in normal variables. *Biometrika*, 48(3/4):419–426, 1961.
- 23 J Gil-Pelaez. Note on the inversion theorem. *Biometrika*, 38(3-4):481–482, 1951.
- 24 Robert B Davies. Numerical inversion of a characteristic function. *Biometrika*, 60(2):415–417, 1973.
- 25 Egon S Pearson. Note on an approximation to the distribution of non-central  $\chi^2$ . *Biometrika*, 46(3/4):364, 1959.
- 26 Huan Liu, Yongqiang Tang, and Hao Helen Zhang. A new chi-square approximation to the distribution of non-negative definite quadratic forms in non-central normal variables. *Computational Statistics & Data Analysis*, 53(4):853–856, 2009.
- 27 Hong Zhang, Judong Shen, and Zheyang Wu. A fast and accurate approximation to the distributions of quadratic forms of gaussian variables. *Journal of Computational and Graphical Statistics*, 31(1):304–311, 2022.
- 28 Pierre Duchesne and Pierre Lafaye De Micheaux. Computing the distribution of quadratic forms: Further comparisons between the liu–tang–zhang approximation and exact methods. *Computational Statistics & Data Analysis*, 54(4):858–862, 2010.
- 29 Dean A Bodenham and Niall M Adams. A comparison of efficient approximations for a weighted sum of chi-squared random variables. *Statistics and Computing*, 26(4):917–928, 2016.
- 30 BK Shah and CG Khatri. Distribution of a definite quadratic form for non-central normal variates. *The Annals of Mathematical Statistics*, pages 883–887, 1961.

## Supplementary information



method	smallest prob.		time/point
	lower	upper	
ncx2cdf	$10^{-308}$	$10^{-18}$	0.2 ms
IFFT	$10^{-3}$	$10^{-5}$	3 ms
ray (dp, $10^3$ rays)	$10^{-5}$	$10^{-308}$	0.5 ms
ray (vp, $10^3$ rays)	—	$10^{-3 \times 10^8}$	23 s

**Figure S1:** The cdf of a non-central chi-square  $\chi_{k=4, \lambda=5}^2$  computed with Matlab's `ncx2cdf`, our IFFT method (with a grid of  $N = 5 \times 10^5$  points that spans 100 times the range over which the cdf is being computed), and our ray-trace method with double precision (open circles) and variable precision (filled), similar to fig. 3. We plot the lower tail probability (cdf) till the median (dashed vertical line), and upper tail probability (complementary cdf) beyond it. The middle of the distribution, probabilities  $> 0.001$  (yellow area) is in linear axes, and the tail regions (green) are in double log axes. The vertical and horizontal white stripes are breaks in the axes, to be able to show the end of the upper tail in the bottom-right, which is much farther below. `realmin` =  $10^{-308}$  is the double-precision limit, and `symmin`  $\approx 10^{-3 \times 10^8}$  is the variable-precision limit. Any missing dots are where a method wrongly computes the tail probability as 0. The table below shows the orders of the smallest lower (finite) and upper (infinite) tail probabilities reached by the different methods with their respective settings, and their computation times per point. 'dp' and 'vp' mean double and variable precision. `ncx2cdf` implements a straightforward calculation for the special case of the non-central chi-square, whereas IFFT and ray-trace are using their full general-purpose algorithm even in this special case, so are expected to take longer. In summary, for non-central chi-square cdf's, `ncx2cdf` is the best method for the lower tail and center, but in the upper tail the ray method is best.